Spectroscopy of C_{60} single molecules: the role of screening on energy level alignment

Isabel Fernández Torrente, Katharina J Franke and Jose Ignacio Pascual

Institut für Experimentalphysik, Freie Universität Berlin, Arnimallee 14,
14195 Berlin, Germany

Abstract
In this paper we investigate the electronic properties of single molecules by means of
low-temperature scanning tunneling spectroscopy (STS). We focus on C_{60} molecules deposited
on a Au(111) surface at different substrate temperatures and mixed with two different
hydrocarbons. In this way we change the fullerene interaction with the surface and/or the
dipolar response of the molecular neighborhood to charging events. We explore the dependence
of the energy level alignment on the molecular surroundings. The results confirm an already
established picture in photoelectron spectroscopy.

(Some figures in this article are in colour only in the electronic version)

1. Introduction

The electronic, optical, thermal, transport, etc., properties of molecular thin films are, in many cases, strongly dependent on properties of the individual entities that constitute the film. Investigation of local phenomena at the molecular scale is thus a challenging research topic, which has been followed up in recent decades due to the development of scanning tunneling microscopy (STM) [1]. STM, as a microscopy tool, was soon applied to investigate the growth and structure of molecular layers [2], especially at the interface with a metal surface. There, STM has allowed us to explore various fields of research in classical chemistry, like conformational dynamics, molecular recognition, coordination and supramolecular chemistry, etc, in a two-dimensional work-bench formed by molecular ensembles adsorbed on a surface [3]. The result is a visualization of molecular aggregation [4, 5] and ordering [6–8], helping us to provide a better understanding of surface chemistry routes required for the formation of functional molecular thin films.

A metal surface plays an important role in the dynamics of thin film growth and in its functionality. First, it acts as a planar support. It also forces molecular motion into a plane, hinders partially intramolecular motion, and, in many cases, interacts chemically with the molecular overlayer. Second, the interface with the metal strongly modifies the individual properties of the molecule, rapidly quenches the excitations, and provides an infinite source/drain of charge [9]. Hence, the molecule on

the metal cannot be considered as an individual entity itself but as a complex system in which the type of external interaction with the surface and its neighbors becomes an important factor to consider.

To investigate such information at the local scale, the spectroscopic mode of the STM plays an important role, since it allows us to resolve the local electronic [10], magnetic [11–13], and vibrational [14] properties of a single molecule. In scanning tunneling spectroscopy (STS) the differential conductivity (dI/dV) of a single molecule junction is measured as a function of tip–sample bias. Variations of dI/dV can be associated with changes in the density of states (DoS) of the molecule/sample electrode, in the magnetic state of a molecule or in the activation of inelastic tunneling processes mediated by molecular vibrations. Depending on the mechanism responsible for the change of the dI/dV signal, different types of information can then be obtained with submolecular resolution. Special mention is due to the inelastic processes occurring during electron tunneling, which may also mediate secondary effects like molecular motion [15–17], dissociation [18, 19], intramolecular dynamics [20, 21], or even the emission of light [22].

In this paper we will analyze an important aspect of local electron spectroscopy regarding to the resolution of the electronic configuration of single molecules: the role of a polarizable neighborhood around a single molecule. In general, dI/dV spectra are directly related to the electronic structure of the molecule/surface system, and it is currently

1

used to determine the alignment of molecular levels with respect to the Fermi level (E_F) as well as their line shape, providing information about the charge state [23, 24], distortions, and interactions at the local scale. It has been shown that the adsorption site [25, 26] and orientation [27] may also strongly affect the alignment and line shape of molecular resonances, as revealed by their spectral fingerprint in STS data. But not much is known yet about screening effects in the molecular layer.

Since STS explores electronic levels using electrons, it is expected that final-state type effects are important. As an electron spectroscopy, STS should be directly related to other techniques like photoelectron spectroscopy (PS), inverse PS (IPS), and near edge x-ray adsorption spectroscopy (NEXAFS). It is known from photoemission experiments [28–34] that screening effects by neighboring molecules and by image charges at the metal surface are important, and may change the measured alignment of unoccupied levels by large amounts. At a local scale, this means that the level alignment of a single molecule (hereafter always referred to with respect to the metal surface Fermi level E_F) as detected by STS must depend on the molecular neighborhood.

Our study here will compare various results for the energy level alignment of C_{60} molecules adsorbed on Au(111) under different conditions of screening by the surroundings. We use STS to find the position of the unoccupied molecular resonance, and find that it varies by several hundred meV depending on the molecular neighborhood. Such changes in the level alignment are larger than those induced by differences in molecular orientation or adsorption site [25–27]. As we shall show, they can be qualitatively understood from a simple model of screening of tunneling electrons by both image charges at the surface and by surrounding molecules.

In this paper we first introduce the experimental procedure, followed by a general description of charge screening at the molecule/metal interface. Experimental results for C_{60} molecules and molecular structures composed of C_{60} mixed with non-planar hydrocarbons are presented in section 4. All results are compared and summarized in section 5.

2. Molecular system and experimental details

Our study of energy level alignment is performed on C_{60} because this molecule maintains a fairly unperturbed electronic configuration upon adsorption. Due to its high symmetry, molecular orbitals are largely degenerate. In particular, the highest occupied and lowest unoccupied molecular orbitals (HOMO and LUMO) have a degeneracy of 5 and 3, respectively. In our study we focus on resolving the shape and alignment of the LUMO and the HOMO–LUMO energy gap, hence taken as a fingerprint of the local molecular properties. C_{60} is co-adsorbed with two different types of hydrocarbons with a three-dimensional shape, with the aim of varying both the properties of the local molecular neighborhood and, as we shall demonstrate, the distance between the fullerene and the metal surface [5].

We use a Au(111) surface as the metal substrate throughout this study. In this way energy level alignment can be qualitatively compared between the different systems explored. Fullerene adsorption on Au(111) surfaces has been extensively studied during recent years, producing a wealth of information about structural phases [25, 35–38] and electronic configurations [25, 27–29, 39–42] of the hexagonally ordered C_{60} films. Charge transfer of C_{60} on Au(111) is fairly small, as observed through STS and density functional calculations [40, 43]. Since the LUMO resonance of C_{60} on Au(111) lies far from E_F small changes in its alignment will not alter significantly the charge state of the fullerene, allowing us to interpret level shifts as entirely due to screening effects from the molecular neighborhood and from the underlying metal surface. The structure of supramolecular architectures formed by the combination of C_{60} with different types of flat hydrocarbons have been characterized [44–46], but the electronic properties associated with the embedding of C_{60} in such molecular networks are still under study [47].

The experiments were carried out in a custom-built low-temperature scanning tunneling microscope (STM) working under ultra-high vacuum conditions and at a temperature of 5 K. Both C_{60} and hydrocarbon molecules were deposited using a Knudsen cell onto a Au(111) surface, previously cleaned using standard sputtering–annealing methods. During the deposition process the Au(111) surface can be maintained at a chosen temperature. Co-deposition of two molecular species usually forms multiple mixed phases and bonding structures depending on the substrate temperature during deposition and on the stoichiometry of the components. These degrees of freedom are used in this study to vary the type of molecular neighborhood around the inspected fullerene. After preparation of the molecular film the sample is transferred into the cold STM for its inspection.

Scanning tunneling spectroscopy measurements were performed using a lock-in amplifier to obtain a signal proportional to the differential conductivity (dI/dV) of the tunnel junction. For these measurements the bias voltage was modulated with an amplitude (typically around 10 mV rms) considerably smaller than the peak line width. STM tips are usually prepared by gentle indentations into a bare gold substrate. The electronic structure of the tip was checked by recording background spectra. This requirement was fulfilled for all the spectroscopy data shown here.

3. Role of screening in the energy level alignment

When a charged particle is placed on or removed from a neutral molecule, additional energy U due to the Coulomb repulsion/attraction with other molecular charges has to be given. This is known as the on-site Hubbard energy. The Hubbard energy modifies the molecular levels when measured by electron spectroscopies, resulting in a HOMO–LUMO energy distance larger than in a simple 'one-particle' picture. The HOMO–LUMO gap of C_{60} in this 'one-particle' scenario amounts to a value of $\Delta = 1.6$ eV. This is the energy gap of a neutral molecule. However, the 'real' gap accounting for final state Coulomb effects is 4.95 eV, which is the
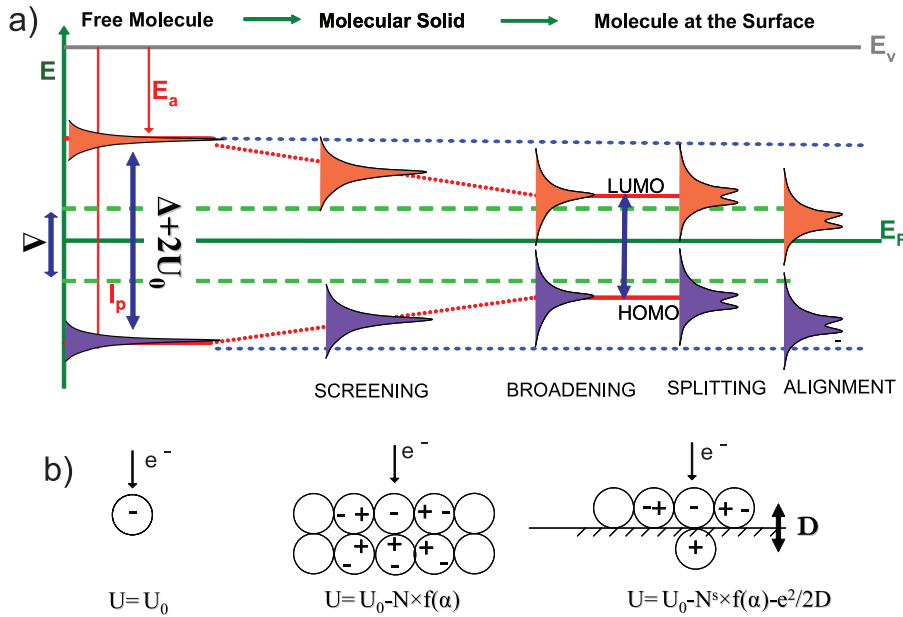
Figure 1. (a) Schematic drawing of the molecular energy level alignment with respect to metal states and the reduction of the charging energy U (b) due to screening by neighboring molecules and by a metal surface. Interaction with a metal can further add broadening, degeneracy splitting and pinning, due to chemisorptive interaction.

difference between the gas phase ionization potential (IP = 7.6 eV) [48–51] and the electron affinity (EA = 2.65 eV) [52]. For simplicity we may assume that the energy costs of electron addition and removal are similar. Then U typically amounts to ~1.7 eV for a free C_{60} molecule [28].

When the fullerene is located in a C_{60} molecular crystal the molecular states overlap with those of neighboring molecules, and their energy line shape broadens [42, 53]. In addition, mobile charge carriers in the neighborhood screen the local charge added to/removed from the fullerene by rearranging their distribution, hence reducing the value of the Hubbard on-site energy (figure 1(a)). This causes the HOMO–LUMO energy gap to be considerably reduced with respect to the free molecule value. For molecular solids like C_{60} intermolecular interactions are non-covalent and weak. The overlap between molecular states is very small, and screening of charges is dominated by the polarizable character of the local neighborhood. According to a simple model, this effect reduces the charging energy by a factor of [54]

$$N \times f(\alpha) = \frac{Ne^2\alpha}{2R^4} \qquad (1)$$

where α is the molecular polarizability [55], R the intermolecular distance and N the coordination number [28].

When the molecular layer is in contact with a metal surface, charge redistribution at the metal–molecule interface can also effectively screen the addition or removal of a charge [28, 56]. The interaction between the charged molecule and its image charge reduces the ionization potential and increases the electron affinity by

$$E_i = \frac{e^2}{2D} \qquad (2)$$

where D is the distance between the charged molecule and its image charge at the surface [28].

In agreement with the above described screening mechanisms, PS + IPS results show that the HOMO–LUMO gap of bulk C_{60} is 3.7 eV [42], while for a C_{60} monolayer in contact with a Au(111) surface this value reduces to 2.3 eV [39]. As we shall show in the next section, the effect of the metallic surface and the molecular neighborhood are also important for understanding the energy level alignment in the final state as seen by STS.

4. Experimental results

4.1. C_{60} on Au(111)

As a reference state, we first probe the STS spectra of an individual C_{60} molecule on a clean Au(111) surface. To obtain isolated C_{60} we deposited the molecules on a cold gold surface at 80 K. At such low temperature, thermally induced molecular diffusion is frozen, thus hindering the self-assembly of molecular clusters. High-resolution STM images find that fullerenes appear isolated in the middle of flat terraces and exhibit a characteristic intramolecular structure composed of lobes (figure 2(a)). The structures resemble the shape of the LUMO constant-DoS isosurfaces, as revealed by density functional calculations for a free C_{60} molecule [57]. The lobes represent the accumulation of DoS around the pentagonal faces of the icosahedral cage. The orbital resolution allow us to see that the molecules may adsorb with different orientations. For example, the internal shapes of the two marked molecules in figure 2(a) fit with a top view of fullerenes with their C2 and C5 symmetry axis lying perpendicular to the surface, as shown in figure 2(c).
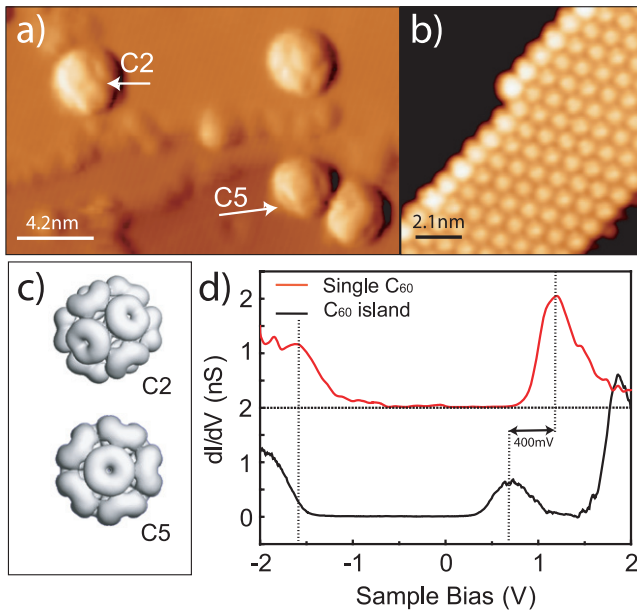
Figure 2. (a) Individual C_{60} molecules as deposited on a cold (80 K) Au(111) surface ($I = 0.13$ nA, $V = 2$ V). The different molecular orientations can be resolved in the intramolecular structure. (b) Hexagonal phase of C_{60} deposited on Au(111) at room temperature ($I = 0.86$ nA, $V = -1$ V). (c) Isosurfaces of constant density of states for the LUMO orbital of free fullerene molecules showing the C2 and C5 symmetry axis [57]. (d) Comparison of STS spectra obtained on the systems shown in (a) (top plot, $I = 1.1$ nA, $V = 2$ V) and (b) (bottom plot, $I = 1.9$ nA, $V = 2.5$ V) [58].

STS measurements were performed on single C_{60} molecules located away from substrate steps. Typical spectra show various features around the Fermi energy which can be related to the alignment of molecular resonances (figure 2(d)). At positive sample bias (above E_F) the peak located at 1.1 eV is associated with the LUMO-derived resonance and shows a peak shape with typically 0.5 eV full width half maximum (FWHM). The HOMO peak usually appears as a shoulder below E_F, and its shape may vary more strongly depending on tip conditions, since at negative sample bias the STS spectra are dominated by the tip's unoccupied electronic structure. However, its position is always around -1.7 eV, hence a HOMO–LUMO gap value of 2.8 ± 0.1 eV is obtained. The alignment of the LUMO peak indicates a negligible charge transfer into C_{60}, as has been also observed and confirmed by DFT calculations in [40].

In order to reveal whether the HOMO–LUMO energy gap is affected by the proximity of neighboring molecules, we compared the spectra obtained on isolated fullerenes with those on C_{60} islands. When C_{60} is annealed on a Au(111) surface at room temperature bi-dimensional islands with hexagonal symmetry [25] are formed (figure 2(b)). The ordered domains are stabilized by weak van der Waals interactions with an average intermolecular distance of 10 Å [35]. The self-assembled structures show various orientational domains, some of which keep a long-range degree commensurate with the underlying Au(111) surface [25, 36, 38].

STS measurements were performed on a C_{60} molecule embedded in one such island, i.e. surrounded by six neighbors.

Under these conditions typical spectra reveal a shift of the unoccupied levels with respect to the spectra obtained for the isolated molecules (figure 2(d)). The LUMO-derived resonance is now located at 0.7 eV. The HOMO feature, on the contrary, does not shift significantly. The HOMO–LUMO gap thus amounts to 2.4 eV, in agreement with other STS measurements [25, 27, 40]. Since C_{60} has a large polarizability due to its 60 π electrons we associate the ~ 400 meV decrease in energy gap with the addition of the six neighboring C_{60} molecules. As we mentioned in section 3, the presence of molecular neighbors with a large polarizability may contribute to reduce the charging energies. To quantify the screening effect of each fullerene we apply equation (1), with an intermolecular distance $R = 10$ Å and a polarizability $\alpha = 90$ Å^3 [54]. According to this relation, the long-range dipolar interaction between two fullerenes amounts to 65 meV. For $N = 6$, this simple approach accounts closely for the experimentally observed shift of the LUMO position.

Other mechanisms may also contribute to modify the LUMO peak alignment. A slight difference in charge transfer depending on the neighborhood could lead to peak shifts. However, it is difficult to quantify this effect since for both single molecules and hexagonal islands we see practically no Fermi level crossing. A different molecular height could also explain a resonance shift due to changes in the distance between the molecule and its image charge. However, in our case this mechanism cannot be proved, because if it exists it would give rise to the opposite effect: fullerenes in the domains should lie higher (if there is any difference) due to lateral interactions with neighbors, and should then be less screened.

4.2. C_{60} + triptycene (TPC) on Au(111)

A further avenue for exploring the role of screening on the molecular energy level alignment is to change the polarizability of the molecular environment by embedding C_{60} in a molecular network with different electronic properties. An appropriate choice for this study is triptycene (TPC). This saturated hydrocarbon consists of a core of two sp^3 hybridized carbon atoms which has attached three phenyl rings giving the molecule a three-dimensional rotor shape (cf figure 3(a)). TPC molecules have a smaller size than C_{60} and are not fully conjugated, thus having a lower polarizability than C_{60} molecules. The concave arrangement of the three phenyl moieties renders this molecule a good candidate to form an inclusion complex with the almost spherical fullerene cage via π–π interactions. This is in fact observed in bulk crystal structures (figure 3(c)) [59–61]. The adsorption of TPC molecules on Au(111) is characterized by a weak molecule–surface bond, as a consequence of the three-dimensional and non-planar molecular structure. Interactions between molecules then become important [62]. As we shall describe in the following section, co-adsorption of C_{60} and TPC leads to the formation of mixed building blocks stabilized by intermolecular forces, in a similar fashion as occurs in bulk.

4.2.1. TPC/C_{60} islands. In order to grow mixed TPC/C_{60} structures we have deposited both molecular species onto
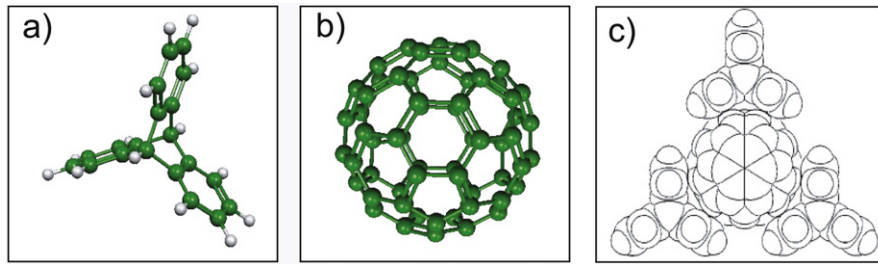
Figure 3. Molecular structure of (a) triptycene ($C_{20}H_{18}$) and (b) C_{60}. (c) Basic building block illustrating the matching of the convex surface of C_{60} into the concave structure of the rotor-shaped molecule TPC. A similar inclusion complex structure is found in the bulk crystal structure [59].

Au(111) at 80 K and, subsequently, annealed to room temperature. When the number of TPC molecules is less than the number of C_{60} a characteristic mixed phase of TPC/C_{60} complexes is found. Figure 4(a) shows a characteristic STM image where the bright protrusions correspond to C_{60} molecules, as identified by their characteristic LUMO shape. The dark, rotor-shaped depressions are associated with TPC single molecules with their threefold symmetry axis oriented perpendicular to the surface. According to this, each of the TPC's concave π moieties bonds to a fullerene, thus leading to the formation of the basic building block indicated by a triangle in figure 4(b). This structure is similar to the bulk inclusion complex and, hence we expect a bonding mechanism mediated by $\pi–\pi$ interactions [59]. Interestingly, the molecular orientation of the fullerenes in the mixed phase appears restricted to orient only with their C3 or C2 symmetry axes perpendicular to the surface, in contrast to the large variety of orientations found in pure C_{60} islands [25, 26, 38]. This fact indicates that some type of local interaction exists between the icosahedral cage and the TPC phenyl rings [63].

An excess of C_{60} molecules leads to the coexistence of both pure fullerene islands and mixed TPC/C_{60} domains with a reduced concentration of embedded TPC molecules. Each TPC molecule bonds with three fullerenes as shown in figure 4(c). This mixed assembly offers the possibility of studying the molecular level alignment of C_{60} with a different number of neighbors. In particular, we find that the LUMO peak shifts upwards with respect to the value in pure C_{60} islands as the number of C_{60} neighbors becomes smaller. A 80 meV shift is found for C_{60} surrounded by five fullerenes (spectrum 2 of figure 4(d)) and two phenyl rings of TPC pointing towards the icosahedral cage. The TPC–C_{60} bonding is thus of H-π character. The comparison of this LUMO shift with the 400 meV displacement observed for the removal of six neighboring fullerenes (i.e. for an isolated C_{60}) suggests that this 80 meV shift can only be attributed to the smaller number of C_{60} neighbors. TPC, in this H-π configuration, hardly plays any role in the screening. The C_{60} marked by dot 3 in figure 4(c) has four C_{60} neighbors. It interacts as well with two TPC molecules, one through a phenyl ring in the just described H-π fashion and another through the two TPC π moieties oriented parallel to the fullerene cage. While the decrease in one fullerene neighbor down to four is expected to yield a further shift of 80 meV, the observed displacement of the
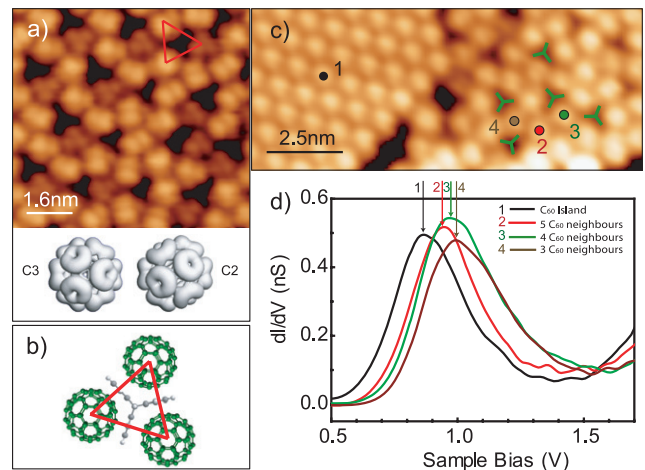

Figure 4. (a) STM image of an ordered structure of TPC/C_{60} after co-deposition at a sample temperature $T_s = 80$ K and annealing to 300 K, ($I = 0.17$ nA, $V = 2.4$ V). Each TPC is surrounded by three fullerenes and this structure is stabilized by $\pi–\pi$ interactions. The triangle indicates the basic building block with its structural model in (b). An excess of C_{60} leads to the formation of pure C_{60} islands and non-stoichiometric mixed islands of TPC and C_{60} as shown in (c). (d) STS characteristics taken on C_{60} molecules with a different molecular environment ($V_{ac} = 16$ mV$_{rms}$, $V = 2.5$ V, $I = 1.2$ nA). The increase (decrease) of TPC (C_{60}) neighbors results in an opening of the gap due to the reduced screening effect of the environment.

LUMO resonance amounts to only 30 meV. We associate this smaller shift with the additional screening of the TPC molecule enclosing the fullerene with the concavely arranged phenyl rings. This $\pi–\pi$ interaction partially compensates the effect of the missing fullerene. A further decrease in the number of neighboring fullerenes by insertion of TPC molecules into the latter geometry (dot 4 in figure 4(c)) leads to an additional shift of the LUMO-derived resonance to higher energies by about 20 meV, a value that is in the same range as the formerly observed 30 meV shift. These results thus confirm that the resonances observed with STS depend critically on the 'local' polarizability of the neighboring molecules.

4.2.2. TPC/C_{60} clusters. In the previous section, we showed that low-temperature co-deposition and room-temperature annealing lead to the expected basic molecular building blocks and the obtained structures have served as an ideal system
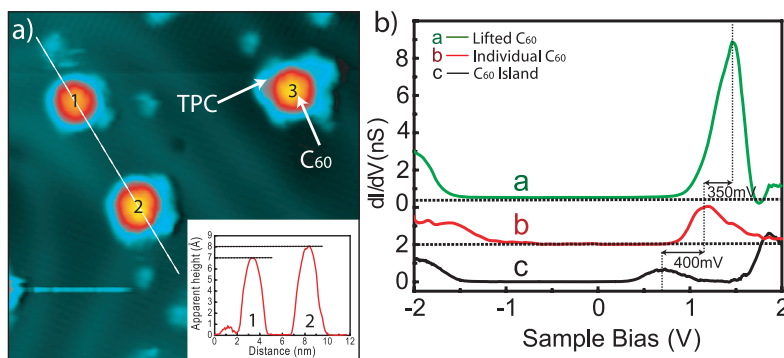
Figure 5. (a) STM image ($I = 0.17$ nA, $V = 2$ V) of a low-coverage co-deposition of C_{60} and TPC at a sample temperature of $T_s = 80$ K. The molecules form small and disordered clusters. A scan profile (inset) through the C_{60} molecules marked as 1 and 2 shows a difference in their apparent height of about 1 Å. (b) STS ($V_{ac} = 26$ mV$_{rms}$, $V = 2$ V, $I = 3.1$ nA) performed on the higher C_{60} (curve a) shows an increase of the HOMO–LUMO gap width of 0.25 eV. This is compared to a single C_{60} (curve b) and C_{60} islands (curve c).

to systematically study the effect of the polarizability of the molecular surrounding. In the observed structures the threefold axis of TPC was oriented perpendicular to the surface, maximizing the π–π interactions to neighboring fullerenes.

Interesting molecular nanostructures are found when small quantities of C_{60} are co-deposited with TPC molecules on a cold surface, at 80 K. At this temperature, C_{60} molecules do not diffuse on the surface acting as nucleation centers for TPC molecules, which exhibit a larger mobility. The result are single fullerene molecules surrounded by lower features, which we associate with TPC molecules assembled in a disordered fashion. Only by slight annealing above 100 K can TPC nucleate in TPC clusters with a well-defined structure and a bandgap of 6 eV [62], but still surrounding the frozen fullerene monomers. Figure 5(a) shows a typical example of such mixed molecular clusters. There, three fullerenes (bright rounded protrusions) appear surrounded by a lower corolla formed by TPC molecules. A ubiquitous observation is that the typical height of C_{60} molecules varies from cluster to cluster. In figure 5(a), fullerenes 2 and 3 appear in the STM images ~ 1 Å higher than fullerene 1 (see inset of figure 5(a)), which shows the standard apparent height usually observed in our experiments (i.e. ~ 7 Å).

Such a height difference could be due to either geometrical or electronic reasons. Regarding the latter, charge transfer between TPC and C_{60}, for example, may lead to changes in the apparent height of the molecules. However, charge transfer should change the apparent height in the opposite sense as observed in our experiment, given the acceptor character of C_{60} and the nucleophilic nature of the phenyl rings. Hence, we tentatively associate the increase in apparent height as being due to the geometrical lifting of the C_{60} cage from the surface as a consequence of the interaction with TPC clusters. This seems to be further corroborated by our STS measurements.

The electronic configuration of molecules 2 and 3 in our dI/dV spectra (figure 5(b)) shows that the LUMO-derived resonance is now located at 1.45 eV, i.e. shifted 350 meV upwards in energy compared to the case of isolated C_{60} molecules shown in figure 2(c). Such an upward shift cannot be explained by the screening caused by the presence of TPC molecules around the fullerene, since this would rather

cause a downward shift with respect to the isolated C_{60} case. Charge transfer can also be discarded from the arguments given above. We can explain the energy shift by considering that the fullerenes are lifted from the surface by their interaction with the surrounding TPC corolla. The increase in molecular distance to the surface reduces the charge screening by the image charges in the metal. According to this, TPC acts as a thin insulating molecular layer between C_{60} and the metal, increasing the charging energy[1] U and, additionally, decreasing the electronic coupling between the fullerene and the surface [64, 65].

4.3. C_{60} + 1,3,5,7-tetraphenyladamantane (TPA) on Au(111)

As a second candidate to interact with a fullerene, we chose 1,3,5,7-tetraphenyladamantane (TPA) (figure 6(a)). Similar to triptycene, its concave carbon skeleton makes this three-dimensional hydrocarbon a suitable molecular partner to form an inclusion complex with the curved conjugated carbon cage of C_{60}. Moreover, the TPA HOMO–LUMO gap is about four times as large as that of C_{60}. Due to this large difference in gap we expect no intermolecular hybridization of the frontier orbitals. Hence, the energy level alignment and electronic coupling with the surface can be studied, while the TPA molecules can be regarded as passive decouplers.

The tetrahedral symmetry of this hydrocarbon results in only one adsorption orientation on a surface. Three phenyl moieties are lying in an almost flat configuration on the substrate, while the fourth one is pointing upwards. STM images this molecule as a circular protrusion with no internal structure. Deposited at room temperature on clean Au(111), TPA shows a variety of adsorption structures depending on its coverage. A weak interaction with the Au surface can be inferred by a large mobility of the molecules under the influence of the STM tip (figure 6(a)). Only steric hindrance between the molecules leads to a stabilization of the molecules into disordered clusters. With increasing coverage, hexagonal 'flower' structures, dimer double rows and finally close packed

---

[1] This effect is probably accompanied by an additional upwards shift of the unoccupied levels as a response to the tip–sample potential drop during the STS measurement [67].
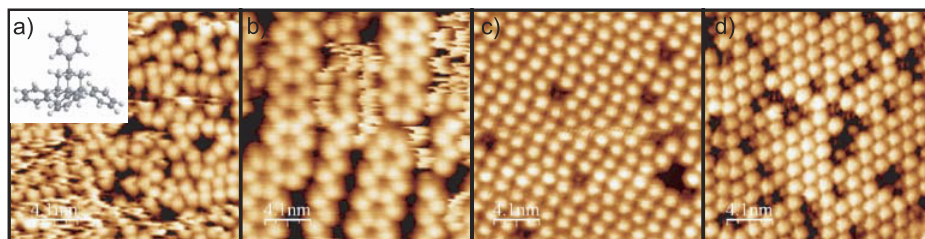
Figure 6. STM images of TPA on Au(111) (inset: molecular structure of TPA): each protrusion corresponds to a single molecule. Under the influence of the STM tip TPA is very mobile, thus leaving lines along the scanning direction in the images. Only the steric hindrance avoids further dragging by the STM tip. At very low coverage ($\sim$0.2 ML) this results in disordered clusters (a). Increasing coverage ($\sim$0.4 ML) leads to hexagonal 'flower' arrangements (b), a dimer row structure ($\sim$0.9 ML) (c), and hexagonal closed packed islands ($\sim$1.0 ML) (d). Scanning conditions: $I = 4$ pA, $V = 870$ mV.
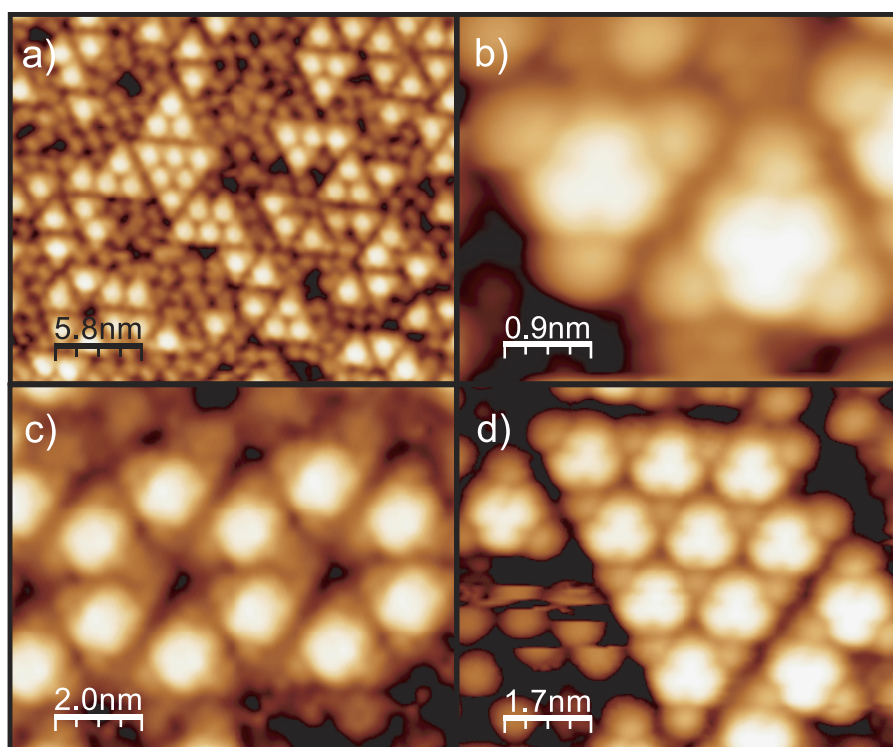

Figure 7. STM images after deposition of C_{60} onto a TPA ($\sim$0.5 ML) pre-covered Au(111) surface. (a) Large scale overview ($I = 0.014$ nA, $V = 860$ mV). (b) Smallest TPA/C_{60} complexes ($I = 0.025$ nA, $V = 870$ mV). (c) Self-assembled structures of TPA/C_{60} tetramers ($I = 0.014$ nA, $V = 860$ mV). (d) Periodically extended structure of TPA/C_{60} ($I = 0.025$ nA, $V = 870$ mV). All images reveal that each fullerene is in the same local arrangement. The C_{60} is always oriented with a C3 axis perpendicular to the surface.

hexagonal islands can be found (figures 6(b)–(d)). These pre-covered surfaces have then been used as a template for additional C_{60} deposition at room temperature.

4.3.1. Lifting and locking the orientation of C_{60} in TPA/$(C_{60})_3$ tetramers. For a pre-coverage of about 0.5 ML of TPA and subsequent deposition of C_{60}, figure 7(a) shows a representative overview of the obtained molecular structures. Most prominent in these images are triangular-shaped arrangements, which can be attributed to TPA/C_{60} mixed nanostructures. The smallest unit of these nanostructures (close-up view in figure 7(b)) consists of one C_{60} molecule, as can be identified from the characteristic threefold LUMO shape, surrounded by three TPAs, imaged as lower protrusions

at the vertices of the triangle. These tetramers serve as stable building blocks for larger self-assembled molecular structures, such as the hexagon in figure 7(c) and the periodically extended structure in figure 7(d). Interestingly, the orientation of the fullerene cage is always the same in the TPA/C_{60} complexes. This observation is opposed to pure C_{60} molecular islands on Au(111), which are also occasionally found. Here, the C_{60} adopts many different molecular orientations (as shown in section 4.1) [25, 38, 40]. Similar to the finding in the TPC/C_{60} mixed phase, the locking of the fullerene cage in the TPA/C_{60} complexes into a particular orientation suggests a local interaction between the molecules [5, 63].

In order to resolve the electronic structure of C_{60} embedded in the TPA triangles, we measure the differential
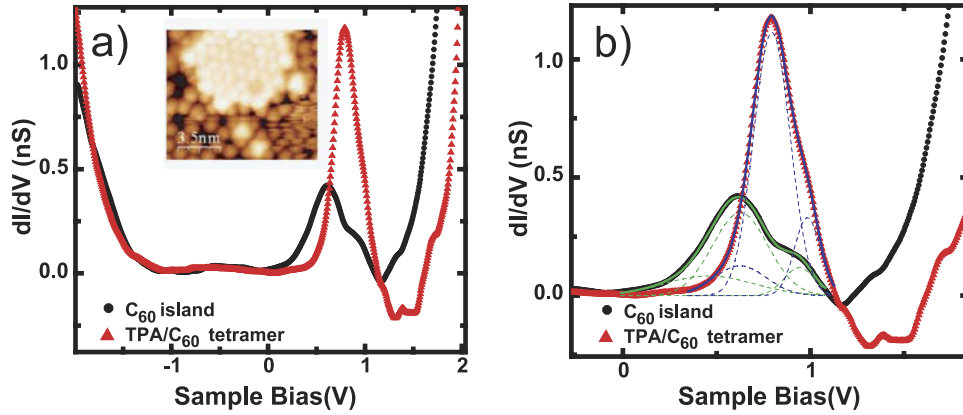
Figure 8. (a) $dI/dV-V$ curves ($V_{ac} = 7$ mV$_{rms}$, $V = 2.3$ V, $I = 1.1$ nA) recorded on a TPA/C$_{60}$ tetramer (red, triangles) and on a pure C$_{60}$ island (black, circles) (see inset). The LUMO of C$_{60}$ in the islands is found at $\sim$630 meV with an overall width of $\sim$ 480 meV, while the C$_{60}$ in the tetramers exhibits the LUMO with negative differential resistance (NDR) at $\sim$810 meV with a smaller width of $\sim$290 meV. (b) The LUMO lineshapes are fitted by three Gaussians (dashed lines). In a pure C$_{60}$ island these are centered at 460, 640, and 940 meV with FWHM of 480, 300, and 160 meV, respectively. A smaller splitting (Gaussians centered at 630, 800, and 990 meV) and smaller FWHM (280, 200, and 140 meV) are found in the C$_{60}$ in the tetramers.

conductance characteristics. A typical dI/dV spectrum of TPA/C$_{60}$ complexes is presented in figure 8. The feature at -1.7 eV is associated with the C$_{60}$ HOMO-derived resonance, while the peak at 0.9 eV represents the LUMO. In figure 8 the spectrum on the tetramers is compared with that obtained on pure C$_{60}$ islands for the same region. On the tetramers the gap width is enlarged and the LUMO position shifted by $\sim$0.2 eV to higher energies. As has been discussed throughout this study, we interpret the shift of the LUMO resonance as related to a less effective screening effect, here by both the substrate and the different molecular neighbors, thus leading to a larger Coulomb repulsion of the tunneling electron.

To get more insight into the C$_{60}$–surface interactions, we compare in figure 8(b) the line shapes of the LUMO-derived resonance in pure C$_{60}$ islands with those in TPA/C$_{60}$ nanostructures. The overall line width of the LUMO-derived resonance in the islands amounts to FWHM $\sim$ 490 meV, while in the nanostructures it is considerably sharper (FWHM $\sim$ 290 meV). As confirmed by DFT calculations of this system in [5] the broadening reflects the hybridization with substrate states, which is considerably reduced when C$_{60}$ is embedded in the TPA/C$_{60}$ tetramers. Moreover, in order to reproduce the line shapes we need to fit the LUMO resonance by three Gauss curves, each of them representing one of the three (in the gas phase degenerate) LUMO levels. Due to the adsorption, the fullerene cage is slightly distorted, leading to symmetry breaking and hence to a loss in the LUMO degeneracy, which can be observed as a splitting in the dI/dV spectra. C$_{60}$ molecules locked by three surrounding TPA, on the other hand, exhibit much less splitting, indicating that the molecular cage is almost restored to its free molecule-like shape. The DFT simulations of [5] further show that the projected density of states (PDOS) onto C$_{60}$ molecular orbitals in C$_{60}$ islands is strongly distorted due to broadening and splitting of the molecular states. In the TPA/C$_{60}$ nanostructures, the cage is deformed by less than 1 pm and the threefold degeneracy of the LUMO is preserved, in agreement with the experimental results.

The most characteristic difference found in the dI/dV spectra of pure C$_{60}$ and TPA/C$_{60}$ complexes is a regime of NDR in the high-energy part of the LUMO. NDR in tunneling dI/dV spectra is known as a fingerprint of localized states weakly coupled with the supporting electrode [64, 66]. We illustrate this effect in figure 9. The tunneling current is resonantly increased when the Fermi level of the tip is aligned with the LUMO level of C$_{60}$. With further increasing bias voltage, elastic tunneling from tip states near the Fermi level is inhibited, while tip states aligned with the LUMO resonance see a larger effective tunneling barrier. If the LUMO resonance is sufficiently sharp, the total tunneling current is thus reduced with increasing bias, resulting in NDR in the dI/dV spectra. Due to the exponential dependence of the tunneling current on barrier height, the NDR effect becomes more pronounced when the tip is retracted from the sample[2]. The observation of NDR in the TPA/C$_{60}$ nanostructures therefore reflects the presence of a sharp LUMO resonance.

We have thus ample experimental evidence that the electronic coupling between the C$_{60}$ molecule and surface is significantly reduced in the TPA/C$_{60}$ nanostructures as compared to C$_{60}$ on Au(111) alone: (i) the HOMO–LUMO gap is enlarged by $\sim$0.2 eV, (ii) the LUMO-derived resonance preserves its degeneracy, (iii) the overall LUMO linewidth is substantially reduced, and (iv) NDR at the high-energy edge of the LUMO. DFT simulations [5] find that the fullerenes in the TPA/C$_{60}$ tetramers are slightly lifted (0.58 Å) from the surface with respect to the case without TPA molecules. This is the reason for the more localized electronic structure, reflected in the spectra as sharper LUMO resonances and NDR behavior.

The reason for the lifting of the fullerene cage lies in the nature of the intermolecular interactions between C$_{60}$ and

---

[2] We have shown in a previous publication [5] that NDR increases with increasing tip–sample distance, hence ruling out any other mechanism which might lead to the observed behavior than a reduced coupling with the substrate and the presence of sharp molecular resonances.
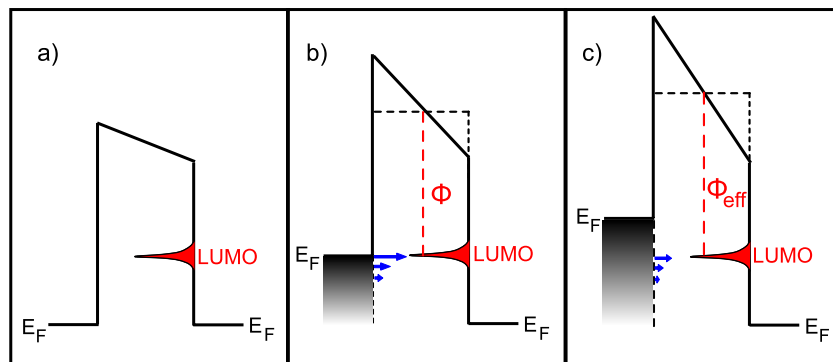
Figure 9. Tunneling barrier exhibiting NDR. (a) Tunneling barrier without applied bias voltage. (b) Tunneling barrier with applied voltage, such that the LUMO is aligned with the Fermi level of the tip, leading to a resonantly increased tunneling current with a tunneling barrier of height Φ. (c) When the bias voltage is further increased and elastic tunneling from tip states near the Fermi level is inhibited, the effective tunneling barrier Φ_{eff} seen by electrons tunneling into the LUMO is larger than in (b) leading to a decrease in tunneling current and hence a negative differential resistance.
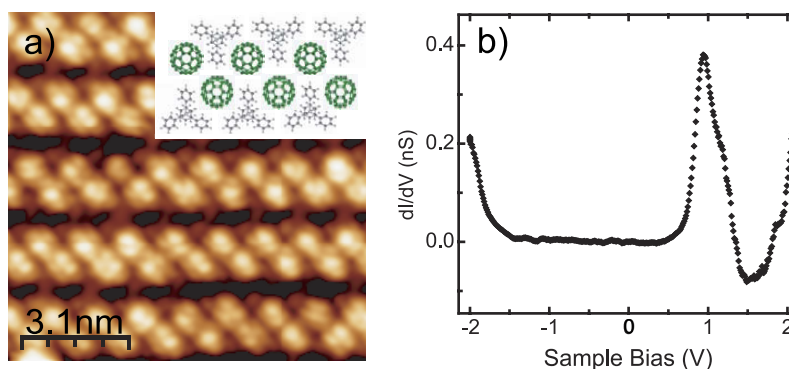

Figure 10. (a) STM image after deposition of C_{60} onto TPA ($\sim$0.9 ML) pre-covered Au(111) ($I = 0.018$ nA, $V = 820$ mV). The main structural unit is double rows of alternating TPA and C_{60} (inset: structural model). (b) $dI/dV-V$ curve ($V_{\text{ac}} = 7$ mV$_{\text{rms}}$, $V = 2.5$ V, $I = 0.5$ nA) recorded on a C_{60} in the row structure. The LUMO is centered at $\sim$900 meV with a FWHM of $\sim$320 meV and shows a clear fingerprint of NDR. Hence, the electronic structure is similar to C_{60} in the tetramers.

TPA. Besides evidencing a reduced coupling to the surface, the LUMO line shape and gap width also exclude a strong chemical interaction between the molecular species, as this would also give rise to broadening effects. Furthermore, we see no features in the dI/dV spectra recorded on TPA in the energy range considered. However, from the STM images we can infer an orientational bonding mechanism, as the C_{60} cage is always exhibiting the same polar and azimuthal orientation with respect to the surrounding TPA. As a possible bonding mechanism we thus consider local electrostatic forces, which imprint the molecular orientation on the C_{60} cage. In contrast to the delocalized nature of van der Waals interactions, hydrogen bonds and electrostatic interactions have a more local and directional character. For the TPA/C_{60} system, DFT calculations find charge accumulation at the H atoms of TPA opposing electron accumulation at the fullerene double bonds. Thus, the fullerene adapts its orientation to maximize the number of electrostatic H··C=C bonds, which concomitantly implies the lifting of the cage from the surface. Although the interactions are weak, the large number of H··C=C bonds that are formed add up to partially compensate the interaction energy between C_{60} and metal surface.

4.3.2. Reduced coupling of C_{60} in one-dimensional molecular rows. While the TPA/C_{60} tetramer structures are most frequently found on the surface with a pre-coverage of 0.5 ML TPA, having a dimer row template of TPA as shown in figure 6(c) (TPA coverage of $\sim$0.9 ML) before C_{60} deposition leads to the formation of double rows of alternating TPA and C_{60} (figure 10). In these structures the fullerene cage exhibits a variety of different orientations. Current–voltage and differential conductance spectra of C_{60} show a similar fingerprint to those in the tetramer arrangement. Again the HOMO–LUMO gap amounts to $\sim$2.6 eV, with the LUMO-derived resonance at $\sim$0.9 eV. The linewidth is $\sim$290 meV and the clear evidence of NDR is also present. Following the arguments of the previous section, we can also deduce a weaker coupling between C_{60} and the surface in this row structure.

The intermolecular interactions leading to this decoupling can be assumed to be of a similar origin as in the tetramer structure. However, the reduced symmetry of the molecular surroundings implies a smaller number of local forces and thus different combinations for the fullerene to lock into two TPA molecules. Moreover, the TPA molecule on the other side of the double row structure probably also plays a role in the stabilization and lifting of the fullerene.
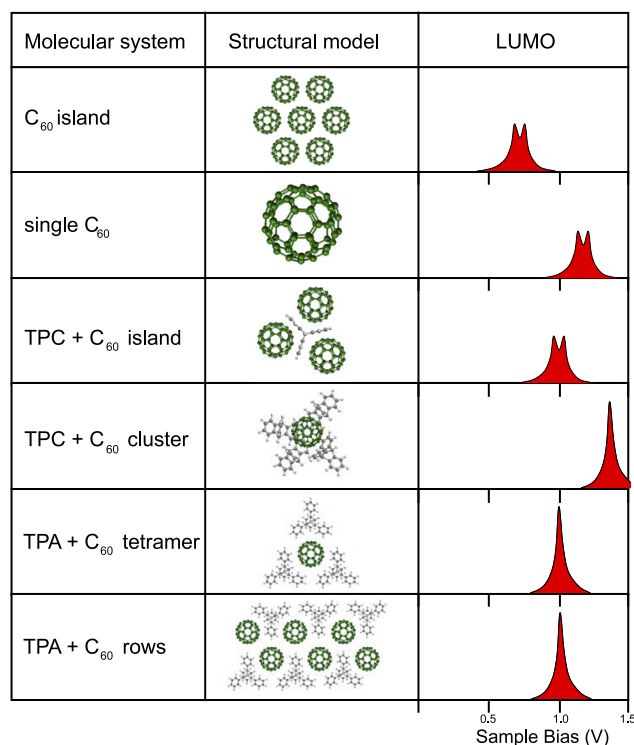
Molecular system	Structural model	LUMO
C_{60} island		
single C_{60}		
TPC + C_{60} island		
TPC + C_{60} cluster		
TPA + C_{60} tetramer		
TPA + C_{60} rows		

Sample Bias (V)

Figure 11. Summary of the C_{60} LUMO splitting and level alignment in the investigated structures.

5. Summary

In our study a single C_{60} molecule has served as a model system for investigating the influence of the molecular environment on the electronic structure. The observed HOMO–LUMO gap obtained in tunneling spectra is a result of the neutral molecule gap plus an on-site Coulomb term due to repulsion of the tunneling electron by electrons in the fullerene cage. This effect can be tuned by polarizable surroundings and we have analyzed it by placing C_{60} in nanostructures of organic molecules on a Au(111) surface. As a reference we started our analysis with isolated fullerenes on Au(111), where the LUMO resonance is found at ∼1.1 eV above E_F. A surrounding of six fullerenes leads to a shift of the LUMO resonance by about 0.4 eV towards the Fermi level, accounting for the large polarizability of about 90 Å^3 of the conjugated carbon cage.

When neighboring molecules of C_{60} are substituted by triptycene, the charge screening is reduced and the LUMO level shifts upwards. This is because triptycene has a lower polarizability than C_{60}. The effect in the LUMO alignment further depends on the orientation of this rotor-shaped molecule with respect to C_{60}: a phenyl ring pointing perpendicular to the fullerene cage thus hardly reduces the on-site Coulomb repulsion of a tunneling electron through the C_{60}. In addition, we have found that the concave arrangement of the phenyl rings of TPC interact via π–π bonding with C_{60} in a similar fashion to bulk, and leads to a more effective screening. We have analyzed the cluster arrangements of one fullerene with various TPCs formed at the Au(111) surface at low temperatures. While the STM images cannot give direct

evidence of the cluster structure, the electronic level alignment hints that the fullerene molecule is lifted from the surface. The LUMO level is found at a bias voltage of ∼1.4 V, a value which is larger than for isolated fullerenes, thus indicating a smaller screening from the metal surface. Moreover, the resonance is narrower and not split, indicating a loss of hybridization with substrate states.

While this cluster structure is not thermodynamically stable, three TPA molecules have been shown to form stable tetramers with C_{60}. In this threefold symmetric structure electrostatic forces are responsible for lifting the fullerene from the surface, thus leading to a reduced coupling which is evidenced in the tunneling spectra as a sharp LUMO resonance and NDR. The level alignment at ∼0.9 eV above the Fermi level accounts for the reduced screening from the metal but some screening from the TPA. The reduced coupling with the metal surface is also found when the fullerness are embedded in a double row structure of alternating TPA and C_{60}.

In summary, we have shown the influence of the screening both from neighboring molecules as well as from the surface on the LUMO level alignment on Au(111). In addition to the screening, adsorption of C_{60} on a metal surface leads to hybridization and a lifting of the degeneracy of the LUMO, both revealed by a broadening of the resonance structure in the STS spectra. A compilation of the results is shown in figure 11.

Acknowledgments

References

[1] Binning G and Rohrer H 1987 *Rev. Mod. Phys.* **59** 615
[2] Ohtani H, Wilson R J, Chiang S and Mate C M 1988 *Phys. Rev. Lett.* **60** 2398
[3] Barth J V, Costantini G and Kern K 2005 *Nature* **437** 671
[4] Böhringer M, Morgenstern K, Schneider W-D, Berndt R, Mauri F, De Vita A and Car R 1999 *Phys. Rev. Lett.* **83** 324
[5] Franke K J, Schulze G, Henningsen N, Fernandez-Torrente I, Pascual J I, Zarwell S, Rück-Braun K, Cobian M and Lorente N 2008 *Phys. Rev. Lett.* **100** 036807
[6] Pawin G, Wong K L, Kwon K Y and Bartels L 2006 *Science* **313** 961
[7] Schickum U, Decker R, Klappenberger F, Zoppellaro G, Klyatskaya S, Ruben M, Silanes I, Arnau A, Kern K, Brune H and Barth J V 2007 *Nano Lett.* **7** 3813
[8] Stepanow S, Lin N, Payer D, Schlickum U, Klappenberger F, Zoppellaro G, Ruben M, Brune H, Barth J V and Kern K 2007 *Angew. Chem. Int. Edn* **46** 710
[9] Fernandez-Torrente I, Monturet S, Franke K J, Fraxedas J, Lorente N and Pascual J I 2007 *Phys. Rev. Lett.* **99** 176103
[10] Li Y Z, Chander M, Patrin J C, Weaver J H, Chibante L P F and Smalley R E 1992 *Phys. Rev.* B **45** 13837
[11] Zhao A D, Li Q X, Chen L, Xiang H J, Wang W H, Pan S, Wang B, Xiao X D, Yang J L, Hou J G and Zhu Q S 2005 *Science* **309** 1542

[12] Iancu V, Deshpande A and Hla S W 2006 *Phys. Rev. Lett.* **97** 266603

[13] Iancu V, Deshpande A and Hla S W 2006 *Nano Lett.* **6** 820

[14] Stipe B C, Rezaei M A and Ho W 1998 *Science* **280** 1732

[15] Stipe B C, Rezaei M A and Ho W 1998 *Phys. Rev. Lett.* **81** 1263

[16] Komeda T, Kim Y, Kawai M, Persson B N J and Ueba H 2002 *Science* **295** 2055

[17] Pascual J I, Lorente N, Song Z, Conrad H and Rust H P 2003 *Nature* **423** 525

[18] Stipe B C, Rezaei M A, Ho W, Gao S, Persson M and Lundqvist B I 1997 *Phys. Rev. Lett.* **78** 4410

[19] Hla S W, Bartels L, Meyer G and Rieder K H 2000 *Phys. Rev. Lett.* **85** 2777

[20] Liljeroth P, Repp J and Meyer G 2007 *Science* **317** 1203

[21] Henningsen N, Franke K J, Torrente I F, Sehulze G, Priewisch B, Ruck-Braun K, Dokic J, Klamroth T, Saalfrank P and Pascual J I 2007 *J. Phys. Chem.* C **111** 14843

[22] Qiu X H, Nazin G V and Ho W 2003 *Science* **299** 542

[23] Wachowiak A, Yamachika R, Khoo K H, Wang Y, Grobis M, Lee D H, Louie S G and Crommie M F 2005 *Science* **310** 468

[24] Repp J, Meyer G, Paavilainen S, Olsson F E and Persson M 2006 *Science* **312** 1196

[25] Rogero C, Pascual J I, Gomez-Herrero J and Baro A M 2002 *J. Chem. Phys.* **116** 832

[26] Silien C, Pradhan N A, Ho W and Thiry P A 2004 *Phys. Rev.* B **69** 115434

[27] Schull G, Néel N, Becker M, Kröger J and Berndt R 2008 submitted
Schull G, Néel N, Becker M, Kröger J and Berndt R 2008 private communication

[28] Hesper R, Tjeng L H and Sawatzky G A 1997 *Europhys. Lett.* **40** 177

[29] Hesper R 2000 The influence of surfaces and interfaces on the properties of C_{60} compounds *PhD Thesis* University Groningen

[30] Lang N D and Kohn W 1973 *Phys. Rev.* B **7** 3541

[31] Ischii H, Sugiyama K, Ito E and Seki K 1999 *Adv. Mater.* **11** (8) 605–25

[32] Kahn A, Koch N and Gao W 2003 *J. Polym. Sci.* B **41** 2523–48

[33] Zaremba E and Kohn W 1976 *Phys. Rev.* B **13** 2270

[34] Koch N, Kahn A, Ghijsen J, Pireaux J-J, Schwartz J, Johnson R L and Elschner A 2003 *Appl. Phys. Lett.* **82** 70

[35] Altman E I and Colton R J 1993 *Phys. Rev.* B **48** 18244–9

[36] Altman E I and Colton R J 1993 *Surf. Sci.* **295** 13–33

[37] Gaisch R, Berndt R, Gimzewski J K, Reihl B, Schlittler R R, Schneider W D and Tschudy M 1993 *Appl. Phys.* A **57** 207

[38] Schull G and Berndt R 2007 *Phys. Rev. Lett.* **99** 226105

[39] Hoogenboom B W, Hesper R, Tjeng L H and Sawatzky G A 1998 *Phys. Rev.* B **57** 11939

[40] Lu X H, Grobis M, Khoo K H, Louie S G and Crommie M F 2004 *Phys. Rev.* B **70** 115418

[41] Tzeng C T, Lo W S, Yuh J Y, Chu R Y and Tsuei K D 2000 *Phys. Rev.* B **61** 2263

[42] Ohno T R, Chen Y, Harvey S E, Kroll G H, Weaver J H, Haufler R E and Smalley R E 1991 *Phys. Rev.* B **44** 13747

[43] Schulze G, Franke K J and Pascual J I 2008 *New J. Phys.* arXiv: 0803.2222v1

[44] Gimzweski J K, Jung T A, Cuberes M T and Schlittler R R 1997 *Surf. Sci.* **386** 101

[45] de Wild M, Berner S, Suzuki H, Yanagi H, Schlettwein D, Ivan S, Baratoff A, Guentherodt H-J and Jung T A 2002 *ChemPhysChem* **10** 881

[46] Spillmann H, Kiebele A, Stöhr M, Jung T A, Bonifazi D, Cheng F and Diederich F 2006 *Adv. Mater.* **18** 275

[47] Wang Y, Yamachika R, Wachowiak A, Grobis M and Crommie M F 2008 *Nat. Mater.* **7** 194

[48] Lichtenberger D L, Nebesny K W, Ray C D, Huffman D R and Lamb L D 1991 *Chem. Phys. Lett.* **176** 203

[49] de Vries J, Steger H, Kamke B, Menzel C, Weisser B, Kamke W and Hertel I V 1992 *Chem. Phys. Lett.* **188** 159

[50] Yoo R K, Ruscic B and Berkowitz J 1992 *J. Chem. Phys.* **96** 911

[51] Hertel I V, Steger H, de Vries J, Weisser B, Menzel C, Kamke B and Kamke W 1992 *Phys. Rev. Lett.* **68** 784

[52] Yang S H, Pettiete C L, Conceiao J, Cheshnovsky O and Smalley R E 1987 *Chem. Phys. Lett.* **139** 233

[53] Weaver J H, Martins J L, Komeda T, Chen Y, Ohno T R, Kroll G H, Troullier N, Haufler R E and Smalley R E 1991 *Phys. Rev. Lett.* **66** 1741

[54] Bonin K D and Kresin V V 1997 *Electric-Dipole Polarizabilities of Atoms, Molecules, and Clusters* (Singapore: World Scientific)

[55] Miller K J and Savchik J A 1979 *J. Am. Chem. Soc.* **101** 7206

[56] Duffy D M and Stoneham A M 1983 *J. Phys. C: Solid State Phys.* **16** 4087

[57] Pascual J I, Gomez-Herrero J, Sanchez-Portal D and Rust H P 2002 *J. Chem. Phys.* **117** 9531–4

[58] All images have been displayed using the WSxM software described in Horcas I *et al* 2007 *Rev. Sci. Instrum.* **78** 013705

[59] Marc Veen E *et al* 1999 *Chem. Commun.* **1999** 1709

[60] Konarev D V, Zubavichus Y V, Valeev E F, Slovokhotov Y L, Shulǵa Y M and Lyubovskaya R N 1999 *Synth. Met.* **103** 2364

[61] Konarev D V, Drichko N V, Lyubovskaya R N, Shulǵa Y M, Litvinov A L, Semkin V N, Dubitsky Y A and Zaopo A 2000 *J. Mol. Struct.* **526** 25

[62] Fernandez-Torrente I, Franke K J, Henningsen N, Schulze G, Alemani M, Roth Ch, Rurali R, Lorente N and Pascual J I 2006 *J. Phys. Chem.* B **110** 20089

[63] Bulusheva L G, Okotrub A V, Gusel'nikov A V, Konarev D V, Litvinov A L and Lyubovskaya R N 2003 *J. Mol. Struct.* **648** 183

[64] Repp J, Meyer G, Stojkovic S M, Gourdon A and Joachim C 2005 *Phys. Rev. Lett.* **94** 026803

[65] Repp J, Meyer G, Paavilainen S, Olsson F E and Persson M 2005 *Phys. Rev. Lett.* **95** 225503

[66] Grobis M, Wachowiak A, Yamachika R and Crommie M F 2005 *Appl. Phys. Lett.* **86** 204102

[67] Datta S, Tian W D, Hong S H, Reifenberger R, Henderson J I and Kubiak C P 1997 *Phys. Rev. Lett.* **79** 2530